Response of Charring Ablators to Severe Aerodynamic and Erosion Environments

R. M. Clever*
Science Applications, Inc., El Segundo, Calif.

and

V. E. Denny†
University of California, Los Angeles, Los Angeles, Calif.

Results of an analytical study for the transient and quasi-steady response of a typical charring ablator to severe aerodynamic and erosion environments are reported for heating loads and particle-surface interactions which are representative of wind tunnel tests as well as re-entry conditions. The coupled erosion-char formation process is shown to be self-limiting, and both discrete and continuous models for erosion of partially charred material, based on experimental data for virgin and fully charred material, are found to give similar results. The numerical solution procedure is illustrated for typical re-entry conditions with cloud and/or dust layers located at altitudes of 50, 35, and 10 kft. Application of simple quasi-steady theory is shown to under-predict total recession.

Nomenclature

A_d = damage area, ft^2
A_i = frequency factor for ith pyrolyzing reaction state, sec^{-1}
c = specific heat, Btu/lb °R
D_p = particle diameter, ft
E_i = activation energy for ith pyrolyzing reaction state, Btu/lb-mole
G = mass exchange factor
h = enthalpy, Btu/lb
H_r = recovery enthalpy, Btu/lb
j = diffusive flux, lb/sec ft^2
k = thermal conductivity, Btu/sec ft °R
L = surface recession, ft
$\dot{L}$ = surface recession rate, fps
$\dot{m}''$ = mass flux, lb/sec ft^2
n_i = reaction order for ith pyrolyzing reaction state
P = penetration depth, ft
P_e = external pressure, atmospheres
q = heat flux, Btu/sec ft^2
$\mathcal{R}$ = universal gas constant, Btu/lb-mole °R
St_h = Stanton number for heat transfer
t, t^* = time, sec
T = temperature, °R
u_e = external velocity, fps
v_v = erosion rate for virgin material, fps
v_∞ = particle velocity, fps
y = coordinate normal to surface, ft
y^* = $y-l$
δ_{50} = depth at which $(\rho-\rho_c)/(\rho_v-\rho_c)=0.5$, ft
$\delta_{i,r}$ = depth at which $(\rho-\rho_c)/\rho_c=0.01$, ft
$\delta_{f,r}$ = depth at which $(\rho_v-\rho)/\rho_v=0.01$, ft
ϵ = emissivity
ϵ_v = $(\rho-\rho_c)/(\rho_v-\rho_c)$
θ = frustrum angle, rad
λ_v = penetration depth for virgin material, ft
ρ = density, lb/ft^3
σ = Stefan-Boltzmann constant, 4.76×10^{-13} Btu/sec ft^2 °R^4
τ = obscuration time, sec

Subscripts

o = at time zero, for zero blowing
∞ = at infinity
c = of char
cw = cold wall
d = damage
e = at the boundary-layer edge
eff = effective
er = due to erosion
g = of gas
h = for heat transfer
i = ith reaction state, ith node point, ith species
j = for virgin or char
p = of a particle
ref = reference
s = of solid
v = virgin material
w = at the wall

Received September 5, 1974; revision received March 27, 1975. Work supported by the Space and Missile Systems Organization (SAMSO) under Air Force Contract FO4701-73-C-0095. The SAMSO Project Officer was Major L.J. Hudak. The assistance of L.E. Dunbar and J.F. Courtney with respect to the formulation of the erosion models and treatment of the surface boundary conditions is gratefully acknowledged.

Index Category: Material Ablation.

*Staff Scientist.

†Associate Professor, Energy and Kinetics Department.

Introduction

THE most general analytical treatment of heat transfer to charring ablators in practical heat-shield applications requires simultaneous solution of the governing conservation equations for the external environment and those for the in-depth response of the ablative material. Usually, the resulting coupled problem is time-dependent as well. In addition, heat-shield shape changes can occur which further complicate analysis of the external problem.

Historically, therefore, it has proved necessary to reduce the scope of a given analysis by introducing simplifying assumptions and by restricting attention to appropriate limiting cases. For example, it is usual practice to represent heat transfer to the ablative surface by means of standard correlations for high-temperature boundary-layer flows, in-

troducing correlation factors for blowing[1,2] and for gas-phase chemical reactions,[3,4] taking cognizance of the effects of shape change on, for example, the locations of the sonic point and transition to turbulence, and assuming negligible temporal storage of thermal energy and unity effective transmissivities for incident thermal radiation in the nongray cold gas-layer near the ablator surface. (For modest turbulent Reynolds numbers and high blowing rates of pyrolysis gas, the latter assumption may incur appreciable error.[5,6]) Further, quasi-steady solutions of the overall problem may be appropriate when vehicles travel at hypersonic speeds and surface recession rates due to ablation and erosion are both steady and large.[7] However, such limiting cases are inappropriate when, for example, erosion is intermittent, as may often be the case when a vehicle passes through discrete clouds and ice or dust layers, or recession rates are small. Finally, it generally is accepted that one-dimensional treatments of the in-depth response of the ablative material are appropriate.

The purpose of the present paper is to report results for an analytical study of ablation under conditions of intermittent erosion, with associated fast transients in recession rates and in-depth response, for typical suborbital entry of an ablative heat-shield. The solution approach is one of coupling a numerical solution of the in-depth thermal decomposition problem to a straightforward correlation for the surface heat transfer which accounts for aerodynamic heating, blockage due to blowing, and thermal radiation. Removal of surface material by erosion is modeled semi-empirically using experimental data for the erosion rates of virgin material and spent char, and assuming linearly weighted rates for intermediate states. The latter procedure proves to be adequate since intermediate surface states are found to be self-limiting.

The physical situation is depicted in Fig. 1, where $y^* = y - L(t)$ represents locations relative to the free surface, $L(t)$ is the surface recession, $\dot{m}_g''$ is the mass flux of pyrolysis gases due to in-depth thermal decomposition, and ρ_v and ρ_c are the densities of virgin ablator and spent char, respectively. The general features of the coupled ablation-erosion problem will be illustrated for a typical charring ablator, simulating typical entry conditions by means of an initial "thermal-soak" period (300→50 kft) followed by intermittent erosion to ground level.

Analysis

Mathematical Model

The in-depth response of a charring ablator involves a strongly coupled set of nonlinear equations governing nonsteady heat transfer, material decomposition, and pyrolysis gas flow. The thermal energy equation is coupled to that for material decomposition via source terms, which account for the effects of transpiration and heat of reaction, and state-dependent material properties. In turn, the equations for local decomposition and overall mass conservation involve temperature-dependent chemical kinetics. Accordingly, the governing equations for energy conservations,[8] material decomposition rate, and pyrolysis gas mass flux are taken as

$$\rho c \frac{\partial T}{\partial t} = \frac{\partial}{\partial y}\left(k \frac{\partial T}{\partial y}\right) + (h_g - h_s)\frac{\partial \rho}{\partial t} + \dot{m}_g'' \frac{\partial h_g}{\partial y} \tag{1}$$

$$\frac{\partial \rho}{\partial t} = -\sum_{i=1}^{N} \frac{(\rho - \rho_c)^{n_i}}{\rho_v} A_i e^{-E_i/\Re T} \tag{2}$$

$$\dot{m}_g'' = -\int_y^\infty \frac{\partial \rho}{\partial t}\, dy \tag{3}$$

where subscripts g and s denote gas and solid, respectively. With $y^* = y - L(t)$, $t^* = t$, and $h_g = \int_{T_o}^{T} c_g dT$, Eqs. (1) and (2) assume the form

$$\rho c \frac{\partial T}{\partial t^*} = \frac{\partial}{\partial t^*}\left(k \frac{\partial T}{\partial y^*}\right) + (h_g - h_s)\frac{\partial \rho}{\partial t} + (\rho c \dot{L} + \dot{m}_g'' c_g)\frac{\partial T}{\partial y^*} \tag{4}$$

$$\frac{\partial \rho}{\partial t^*} = \dot{L}\frac{\partial \rho}{\partial y^*} + \frac{\partial \rho}{\partial t} \tag{5}$$

Boundary and initial conditions for the problem are taken as

$$T(y^*,0) = T_o \text{ and } \rho(y^*,0) = \rho_v \tag{6}$$

at $t^* = 0$,

$$T(y^*,t^*) \to T_o \text{ and } \rho(y^*,t^*) \to \rho_v \tag{7}$$

as $y^* \to \infty$, and

$$-k\frac{\partial T}{\partial y^*}\bigg|_{0-} = \left[-k\frac{\partial T}{\partial y^*} + \sum_i j_i h_i\right]_{0+} - (\dot{m}_g'' + \dot{m}_c'')h_w + \dot{m}_g'' h_g + \dot{m}_c'' h_c - \sigma\epsilon T_w^4 \tag{8}$$

at the ablator surface. Following standard practice, the first term on the right is replaced by $\rho_e u_e St_h (H_r - h_w)$ and normalized with respect to the no-blowing flux $\rho_e u_e St_{h,o}(H_r - h_{w,o})$. The resulting Stanton number and enthalpy ratios, as well as the char mass-loss factor $\dot{m}_c''/\rho_e u_e$, were then corrected using data from Ref. 9.

Thermophysical Properties

For illustrative purposes, a typical charring ablator was chosen for which k_v, k_c, and c varied with temperature as

Table 1 Ablator properties

$T(°R)$	$k_v \times 10^4$ (Btu/sec ft °R)	$k_c \times 10^4$ (Btu/sec ft °R)	c^a (Btu/lb °R)
460	0.95	0.67	0.225
560	1.12	0.79	0.29
660	1.22	0.86	0.32
760	1.30	0.91	0.35
860	1.35	0.94	0.38
960	1.38	0.97	0.40
1460	1.75	1.22	0.50
1960	2.12	1.48	0.52
2460	2.45	1.71	0.53
2960	2.90	2.02	0.54
3460	3.27	2.29	0.55
5000	4.48	3.14	0.55
9000	5.23	3.66	0.55

[a] For many ablators, the difference between the specific heats of virgin and fully charred material is not appreciable and it is reasonable to assume c to be composition independent.

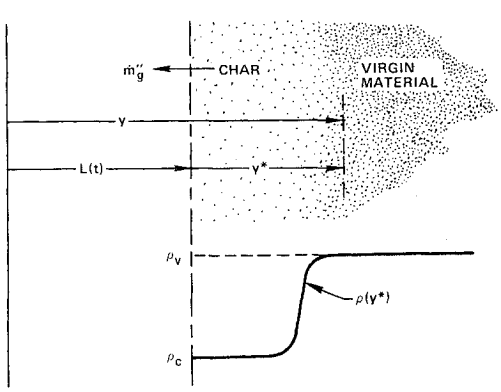

Fig. 1 Schematic of one-dimensional pyrolyzing ablator with surface erosion.

given in Table 1. The densities of virgin and fully charred material were taken as 90.4 and 74.0 lb/ft^3, respectively; while, c_g and $h_g - h_s$ were taken as 0.4 Btu/lb °R and 9300 Btu/lb, respectively. A three legged kinetics expression was used when $n=2$; $E_i = 1208$, 25200, 56041 Btu/lb-mole; and $A_i = 5.1\times10^{-4}$, 85.4, 1.01125×10^{6} sec^{-1} with $i=1$, 2, 3. A simple combining rule for thermal conductivity

$$k = \epsilon_v k_v + (1-\epsilon_v)k_c \tag{9}$$

was selected, where $\epsilon_v = (\rho-\rho_c)/(\rho_v-\rho_c)$.

Solution Method

Equations (2-9) were solved numerically, approximating first and second spatial derivatives by means of implicit, 3-point, central difference analogs and time derivatives as backward difference expressions. Since the results proved to be relatively insensitive to numerical error in $\dot{m}_g''$, the quadrature in Eq. (3) was effected by the simple trapezoidal rule. The resulting coupled set of nonlinear algebraic equations was solved at each time step by means of simple iteration. However, it was found that convergence of the iterative scheme was enhanced upon linearizing the $(h_g - h_s)\,\partial\rho/\partial t$ term in Eq. (4) as well as Eqs. (5) and (8) about previous iterates (^{o}).

$$\frac{\partial\rho}{\partial t} = \left(\frac{\partial\rho}{\partial t}\right)^o + \left[\frac{\partial}{\partial T}\left(\frac{\partial\rho}{\partial t}\right)\right]^o (T-T^o) \tag{10}$$

$$\frac{\partial\rho}{\partial t^*} = \dot{L}\frac{\partial\rho}{\partial y^*} + \left(\frac{\partial\rho}{\partial t}\right)^o + \left[\frac{\partial}{\partial\rho}\left(\frac{\partial\rho}{\partial t}\right)\right]^o (\rho-\rho^o) \tag{11}$$

$$\frac{\partial T}{\partial y^*} = \left(\frac{\partial T}{\partial y^*}\right)^o + \left[\frac{\partial}{\partial T}\left(\frac{\partial T}{\partial y^*}\right)\right]^o (T-T^o) \tag{12}$$

The implicit solution of Eq. (11) merits special attention. As shown in the Appendix, attempts to advance Eq. (11) explicitly, with or without successive iterative advances in $\dot{L}\times(\partial\rho/\partial y^*)$ and $\partial\rho/\partial t$, is inherently unstable for $\Delta t^* > 0(\Delta y^*/\dot{L})$. For small mesh spacings and large erosion rates, therefore, an explicit treatment of Eq. (11) would require prohibitively small time steps. This difficulty was circumvented by approximating $\partial\rho/\partial y^*$ by means of the second-order correct expressions $(\rho_{i+1}-\rho_{i-1})/2\Delta y^*$ for $i>2$ ($y^*>0$), and $(4\rho_3-3\rho_2-\rho_4)/2\Delta y^*$ for $i=2$ ($y^*=0$), giving

$$\rho_2 = A_2\rho_3 + B_2\rho_4 + C_2 \tag{13}$$

$$\rho_3 = A_3\rho_4 + B_3\rho_2 + C_3 \tag{14}$$

etc. On eliminating ρ_4 from Eq. (13) using Eq. (14), there results the set of algebraic equations

$$\rho_i = A_i^*\rho_{i+1} + B_i^*\rho_{i-1} + C_i^* \tag{15}$$

which, with $B_2^* \equiv 0$, yields to simple inversion by means of successive substitution on noting that $\rho_i \to \rho_p$ for i sufficiently large.

Because of the presence of various regimes in a typical reentry environment wherein the thermal and material-decomposition response of an ablating/eroding solid may differ by orders of magnitude, time-dependent nodal systems were assigned in such manner as to constrain the thermal and pyrolysis zone calculations to regions of significant gradients in T and ρ. For the thermal zone, an initial given number $I_{\max}$ of node points was either increased or decreased by N (holding Δy^* fixed) after each time step according to whether

$$q|_{0.75I_{\max}} > N\,q_w\times10^{-4}$$

or

$$q|_{0.75I_{\max}} < 0.75\,q_w x10^{-4}/N$$

respectively. In addition, upper and lower bounds on $I_{\max}$ were imposed such that $I_\ell \le I_{\max} \le I_u$. For the situation in which addition of N nodes would result in $I_{\max} > I_u$, alternate nodes were deleted from the thermal nodal system, $I_{\max}$ being effectively cut in half. For, $I_{\max} < I_\ell$, $I_{\max}$ was approximately doubled by introducing intermediate nodes midway between existing nodes, using quadratic interpolation to assign the corresponding values of T and ρ. Typical values of I_ℓ and I_u were 98 and 200, respectively. In a similar way, a dynamic pyrolysis-zone nodal system was assigned such that $\partial\rho/\partial t > \epsilon_\rho \simeq 10^{-3}$ was maintained. Outside this zone, $\rho=\rho_c$ or $\rho=\rho_v$ as appropriate.

Erosion Modeling

In view of the complex dependence of erosion characteristics on material state, progress on an appropriate model for partially charred ablators dictates that simpifying assumptions be made. Also, the bulk of experimental data available pertains to either virgin or fully charred states, and it proves convenient to model erosion in terms of these limit states. For either limit, therefore, the data admit identification of mass-exchange factors

$$G_j = \dot{m}_j''/\rho_{p\infty}v_\infty\sin\theta \tag{16}$$

where the $\dot{m}_j''$'s are erosion-loss mass fluxes and $\rho_{p\infty}v_\infty\sin\theta$ is the mass flux of incident particles. It further provides convenient to express the $\dot{m}_j''$'s as

$$\dot{m}_j'' = \rho_j P_j/\tau_j \tag{17}$$

where the P_j's are penetration depths for equivalent cavities with uniform cross-sectional areas taken as the surface damage areas $A_{d,j}$ (i.e., $P_j < P_{j,\max}$), and the τ_j's are "obscuration" times, i.e., the times between successive impacts locally. The latter are related to the $A_{d,j}$'s by means of the general expression

$$\tau_j = \rho_p(\pi D_p^3/6)/(A_{d,j}\rho_{p\infty}v_\infty\sin\theta) \tag{18}$$

With the G_j's and the $A_{d,j}$'s known from experiment, the penetration depths for virgin and char are given by

$$P_j = \rho_{p\infty}v_\infty\sin\theta/(\rho_j/G_j\tau_j) \tag{19}$$

A transition-state model for erosion of partially charred material may next be developed in terms of effective penetration depths and damage areas for the case of in-depth variations in material density. The effective penetration depth, P_{eff}, will be established in terms of: 1) the P_j's for virgin and fully charred material; and 2) a presumed functional dependence on P_{eff} on density, an assumption which will prove to have negligible effect on the final results. It is convenient to introduce a dimensionless penetration depth, $P^*(\rho)$, such that $P(\rho) = P_v P^*(\rho)$. The limiting values of P^* are thus 1 for virgin and P_c/P_v for fully charred material. For present purposes, P^* is assumed to decrease linearly with increasing ρ, i.e., increasing depth. The effective penetration depth is now taken as $P_{\text{eff}} = P_v\overline{P^*}$, where $\overline{P^*}$ is an integral average of P^* over the effective penetration depth

$$\overline{P^*} = \int_0^{P_{\text{eff}}} P^*(\rho)\,dy \Big/ \int_0^{P_{\text{eff}}} dy$$

Substituting for $\bar{P}^*$

$$P_{\text{eff}}^2 = P_v \int_0^{P_{\text{eff}}} P^*(\rho)\, dy \tag{20}$$

Similarly, the effective damage area may be determined in terms of 1) the $A_{d,j}$'s and 2) an assumed functional dependence of damage area on either ρ_w or $\bar{\rho}$, the latter being an integral average of ρ over P_{eff}. As before, on introducing a dimensionless damage area A_d^* such that A_d^* decreases linearly with increasing ρ from $A_{d,c}^* = A_{d,c}/A_{d,v}$ to $A_{d,v}^* = 1$, the effective damage area becomes

$$A_{d,\text{ff}} = A_{d,v} A_d^*(\rho) \tag{21}$$

Equations (18-21) are appropriate for modeling *discrete* erosion wherein it is presumed that material to depth P_{eff} is instantaneously removed at intervals τ_{eff}, with τ_{eff} being given by Eq. (18) on replacing $A_{d,j}$ by $A_{d,\text{eff}}$. (After discrete removal, the thermal response problem is re-initialized, the starting in-depth temperature and density distributions being those for $y^* > P_{\text{eff}}$.) For *continuous* erosion, an effective mass-exchange factor

$$G_{\text{eff}} = G_v A_d^* \bar{P}^* \rho_{\text{ref}}/\rho_v \tag{22}$$

is introduced which is used to calculate a continuous erosion recession rate

$$\dot{L}_{er} = G_{\text{eff}} \rho_{p\infty} v_\infty \sin\theta/\rho_{\text{ref}} \tag{23}$$

where ρ_{ref} is taken as either ρ_w or $\bar{\rho} = \int_0^{P_{\text{eff}}} \rho dy \,/P_{\text{eff}}$. Both discrete and continuous erosion are considered here and, as will be shown later, give similar results.

Actually, careful study of the model equations reveal that the erosion mass-loss problem is fully specified in terms of the parameters

$$v_v = G_v \rho_{p\infty} v_\infty \sin\theta/\rho_v \tag{24}$$

and

$$\lambda_v = G_v(\pi/6)\rho_p D_p^3/\rho_v A_{d,v} = \tau_v v_v \tag{25}$$

together with the end-point ratios $G_c^* = G_c/G_v$, $A_{d,c}^* = A_{d,c}/A_{d,v}$, and $\rho_c^* = \rho_v/\rho_c = 1.222$. Physically, λ_v and v_v have dimensions of length and velocity, respectively, and may be viewed as the penetration depth and surface erosion recession rate for virgin material. For the results discussed below, G_c^* and $A_{d,c}^*$ are fixed at 10 and 3, respectively, which are typical values from experiment.

Results and Discussion

Before discussing transient results for typical re-entry conditions with coupled ablation/erosion, it will prove useful to develop the dependence of recession rate ($\dot{L}$) and char depth [δ_{50}, the depth at which $(\rho-\rho_c)/(\rho_v-\rho_c) = 0.5$] on the principal problem parameters, assuming a continuous erosion model throughout and setting $\rho_{\text{ref}} = \bar{\rho}$ in Eqs. (22) and (23). The effects of cold wall heat flux, q_{cw}, and the erosion parameters, v_v and λ_v, on $\dot{L}$ and δ_{50} are displayed in Figs. 2 and 3, with $H_r = 9000$ Btu/lb and $P_e = 30$ atm. From Fig. 2, it is seen that $\dot{L} = \dot{L}_c$ for clean air increases with increasing q_{cw} due to increased thermochemical ablation. As a result, δ_{50} varies inversely with q_{cw} (see Fig. 3) and rapid increases in char depth are to be expected during the early stages of re-entry where q_{cw} typically is small. With erosion, $\dot{L} = \dot{L}_c + \dot{L}_{er}$ is seen to increase with increasing v_v and decreasing λ_v, for given λ_v and v_v, respectively. [From Eq. (25), the latter effect is due to decreases in obscuration time τ_v with λ_v for given v_v.] These effects are more pronouced at reduced q_{cw} since, as shown in Fig. 3, increased char depths admit acceleration erosion of the relatively more friable char. During re-entry, therefore, the effects of erosion would be expected to be more severe for higher cloud or dust layers than for lower ones. Finally, it is seen that the transient times, defined as the times at which $\dot{L} = 0.9 \times \dot{L}_{\text{steady}}$, decrease with increasing q_{cw} and v_v and decreasing λ_v. These effects are summarized in Fig. 4; further properties of the quasi-steady solutions are listed in Table 2. (For discrete erosion, the results are essentially the same, as will be demonstrated later.)

With these points in mind, discussion of the full transient results for a typical re-entry is straightforward. Representative variations in cold wall heat flux and recovery enthalpy with time and altitude are displayed in Fig. 5a, with associated results for $\dot{L}$, δ_{50}, and total recession being given in Fig. 5b, for the case of side-wall heating of an ablating nosetip ($\theta = 9°$). The effects of coupled ablation/erosion are illustrated for a series of three cloud or dust layers of varying thickness at altitudes of 51, 34, and 10.4 kft. As expected δ_{50} increases rapidly during the early stages of re-entry and approaches a quasi-steady value near the peak heating flux. Therefore, δ_{50} undergoes sharp reductions during erosion, followed by modest increases between clouds, and then marked reductions at the reduced heat loads encountered on approaching ground level. The corresponding character of $\dot{L}$ and total recession follow similar trends.

Of interest is the possible application of quasi-steady theory to the estimation, say, of total recession. Unfortunately, this is complicated owing to the broad parametric study required to accommodate the complex variations of H_r, q_{cw}, P_e, and other parameters with altitude. In general, the curve for quasi-steady recession will rise less rapidly than that for the full transient case, relatively larger errors being incurred during periods of erosion since the quasi-steady $\dot{L}$'s will correspond to the reduced values for virgin material. For the example considered here, rough calculations indicate that the quasi-steady results for total recession at the end of the trajectory could be from 10 to 20% low; however, the discrepancy for the stagnation region of the nosetip would be smaller because the heating loads would be higher and the differences between $\dot{L}$ actual and that based on the pure virgin limit would be considerably smaller (see Figs. 2 and 3).

It remains to discuss the relative features of the erosion models and their validity. Although erosion actually involves

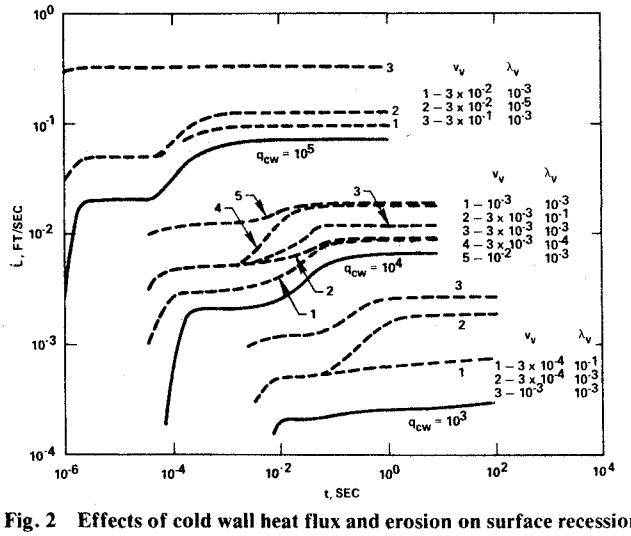

Fig. 2 Effects of cold wall heat flux and erosion on surface recession rate ($P_e = 30$ atm, $H_r = 9000$ Btu/lb).

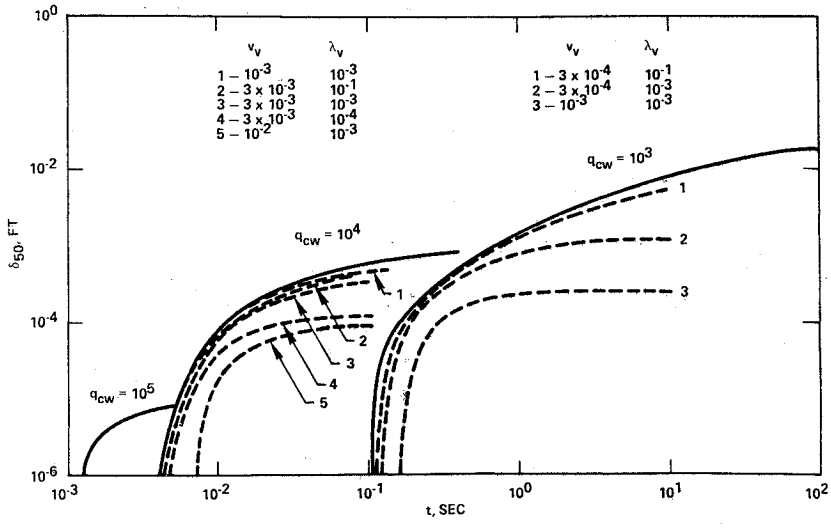

Fig. 3 Effects of cold wall heat flux and erosion on char depth (P_e = 30 atm, H_r = 9000 Btu/lb).

complex and poorly understood mechanics of particle-surface interactions which are at once three-dimensional and time-varying as well as material state dependent, the model approaches adopted here require only that the treatment of intermediate char states be justified since the models conform to experimental data for the virgin and fully-charred states. To this end, the effects of using ρ_w vs the possibly more appropriate $\bar{\rho}$ in the continuous model and comparisons of continuous vs discrete erosion are presented in Fig. 6 for typical values of λ_v, v_v, and q_{cw}. Although use of ρ_w leads to increasingly higher total recession with increasing λ_v than does $\bar{\rho}$ (compare dashed curves), the differences are not excessive. Thus, any arbitrariness introduced in the handling of in-depth material state variations may not incur appreciable error. Further, the results for the discrete and continuous models (compare solid-dashed curves) indicate that either approach is satisfactory, and given added support to the simplifying assumptions envoked since the in-depth material state variations for discrete erosion are relatively more pronounced than are those for continuous erosion. (The reductions in amplitude for the oscillations of the discrete curve about the continuous are due to reductions in obscuration times with increasing damage area as more char forms.)

The principal basis for the relative success of the simple models introduced in the present study is the self-limiting nature of the coupled erosion-char formation process. Since erosion of char is more facile than that for virgin material, any tendency for increased rates for formation of char is

Table 2 Quasi-steady results[a]

		T_w, °R	ρ_w, lb/ft	δ_{50}, ft	L, fps	$\delta_{i,r}$ ft[b]	$\delta_{f,r}$ ft[c]
		6923[d]	80.97	5.91×10^{-6}	7.05×10^{-2}	0	7.34×10^{-5}
Clean		6842	74.13	8.60×10^{-4}	6.49×10^{-3}	4.10×10^{-4}	1.19×10^{-3}
		6225	74.0	2.24×10^{-2}	2.96×10^{-4}	1.89×10^{-2}	2.72×10^{-2}
		...	...	...	...	...	...
	$\lambda=10^{-6}$	6809	74.16	7.40×10^{-4}	7.28×10^{-3}	3.27×10^{-4}	1.02×10^{-3}
		4767	74.07	2.36×10^{-3}	1.47×10^{-3}	1.18×10^{-3}	3.42×10^{-3}
		...	...	...	...	...	...
$v=10^{-4}$	$\lambda=10^{-3}$	6830	74.14	8.16×10^{-3}	6.77×10^{-3}	4.22×10^{-4}	1.14×10^{-3}
		5075	74.03	3.23×10^{-3}	1.26×10^{-3}	1.85×10^{-3}	4.30×10^{-3}
		...	...	...	...	...	...
	$\lambda=10^{-1}$	6838	74.13	8.47×10^{-4}	6.58×10^{-3}	4.10×10^{-4}	1.18×10^{-3}
		6073	74.0	1.32×10^{-2}	4.64×10^{-4}	1.04×10^{-2}	1.60×10^{-2}
		6915	81.41	5.45×10^{6}	7.43×10^{-2}	0	6.70×10^{-5}
	$\lambda=10^{-6}$	6259	74.91	2.56×10^{-4}	1.42×10^{-2}	0	4.34×10^{-4}
		2912	87.38	0	5.88×10^{-3}	0	1.62×10^{-4}
		6921	81.07	8.08×10^{-6}	7.14×10^{-2}	0	7.21×10^{-5}
$v=10^{-3}$	$\lambda=10^{-3}$	6735	74.24	5.76×10^{-4}	8.78×10^{-3}	2.05×10^{-4}	8.19×10^{-4}
		3330	77.88	2.53×10^{-4}	2.71×10^{-3}	0	8.77×10^{-4}
		6921	81.07	8.08×10^{-6}	7.14×10^{-2}	0	7.21×10^{-5}
	$\lambda=10^{-1}$	6807	74.16	7.35×10^{-4}	7.32×10^{-3}	3.23×10^{-4}	1.02×10^{-3}
		4561	74.12	1.91×10^{-3}	1.58×10^{-3}	7.96×10^{-4}	2.89×10^{-3}
		6864	83.75	0	9.81×10^{-2}	0	4.36×10^{-5}
	$\lambda=10^{-6}$	4593	84.93	0	3.14×10^{-2}	0	7.68×10^{-5}
		2500	90.21	0	1.06×10^{-2}	0	0
		6905	81.92	1.83×10^{-6}	7.89×10^{-4}	0	6.14×10^{-5}
$v=10^{-2}$	$\lambda=10^{-3}$	5421	77.28	9.15×10^{-5}	1.90×10^{-2}	0	2.39×10^{-4}
		2525	90.14	0	1.03×10^{-2}	0	0
		6905	81.92	1.83×10^{-6}	7.89×10^{-4}	0	6.14×10^{-5}
	$\lambda=10^{-1}$	6141	75.12	2.24×10^{-3}	1.49×10^{-2}	0	3.96×10^{-4}
		2529	90.13	0	1.03×10^{-2}	0	0

[a] P_e = 30 atm, H_r = 9000 Btu/lb.
[b] Distance at which $(\rho-\rho_c)/\rho_c = 0.01$.
[c] Distance at which $(\rho_v-\rho)/\rho_v = 0.01$.
[d] $q_{cw} = 10^5, 10^4, 10^3$ Btu/sec ft^2.

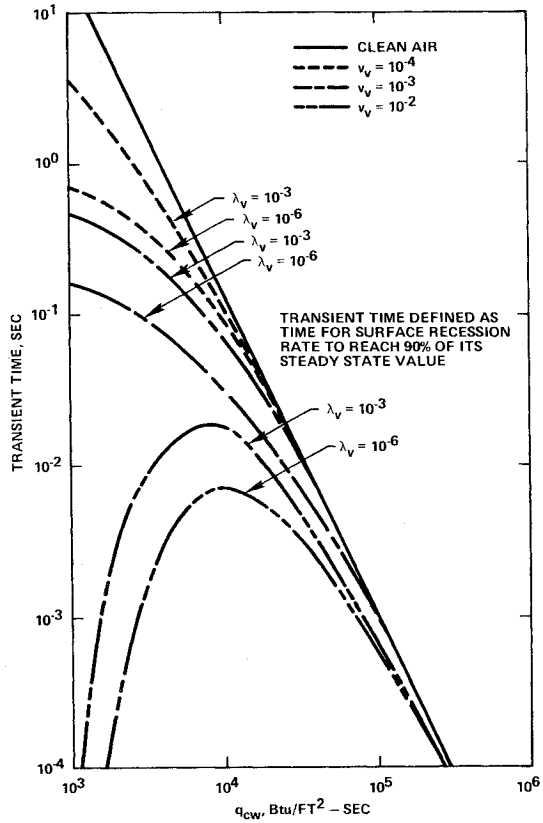

Fig. 4 Transient times for approach to quasi-steady recession ($P_e = 30$ atm, $H_r = 9000$ Btu/lb).

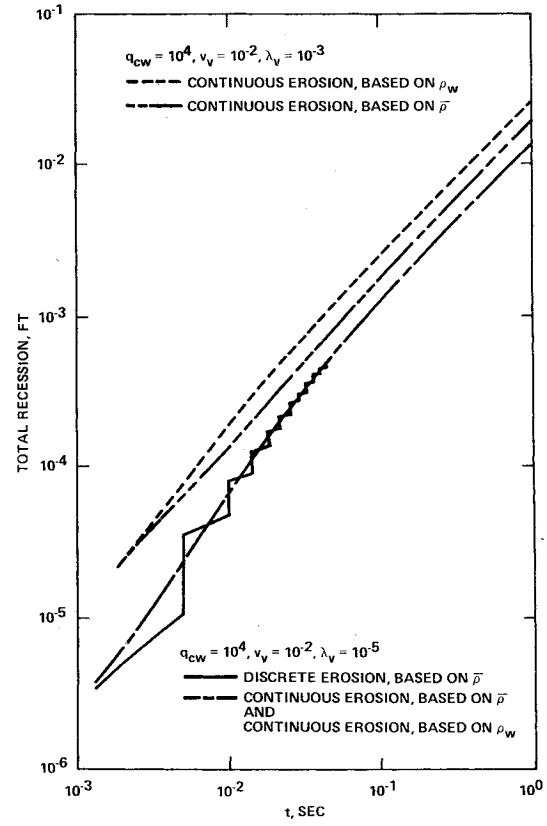

Fig. 6 Comparisons of erosion models for total recession.

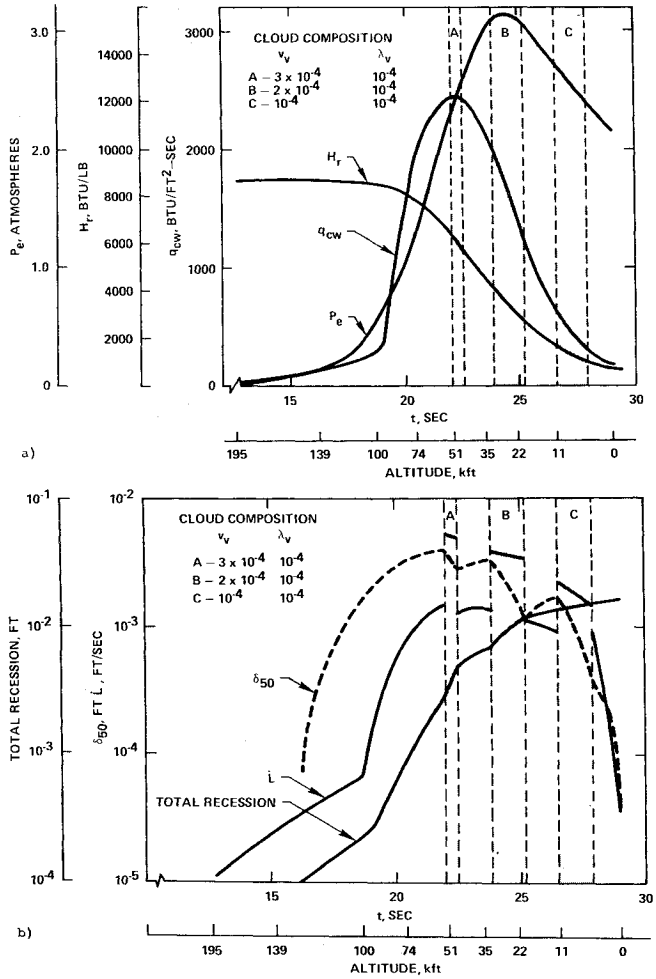

Fig. 5 Typical re-entry. a) environment; b) ablation response.

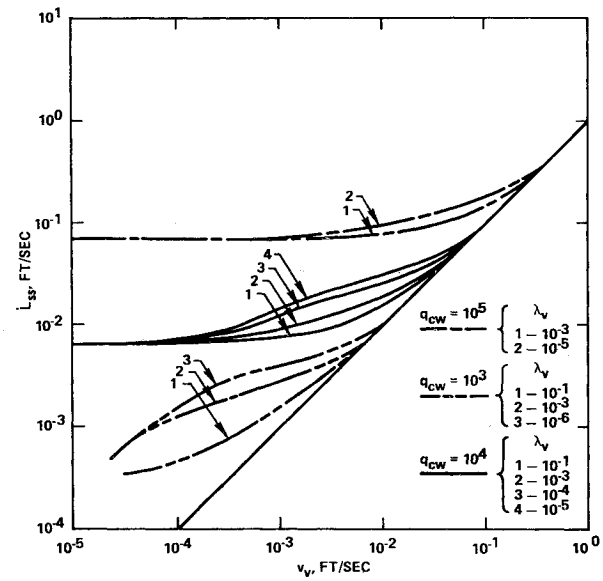

Fig. 7 Effects of erosion parameters on $\dot{L}_{\text{steady state}}$ for continuous erosion ($\rho_{\text{ref}} = \bar{\rho}$].

counteracted by higher erosion rates. This behavior is illustrated in Fig. 7 for a broad range of the problem parameters. For example, an order of magnitude increase in erorion velocity v_v from 10^{-3} to 10^{-2} (with $\lambda_v = 10^{-5}$ and $q_{cw} = 10{,}000$) results in only an approximate two-fold increase in recession rate. (This observation breaks down, of course, for v_v sufficiently large since material state variations no longer are present and $\dot{L}$ asymptotically approaches v_v.)

Conclusions

1) The computational efficiency and stability of finite difference solutions to the partial differential equations gover-

ning in-depth conservation of thermal energy and material decomposition for a pyrolyzing ablator subject to surface erosion and thermo-chemical ablation is enhanced by means of quasi-linearization of the surface thermal boundary condition and material decomposition rate expression and fully implicit finite-differencing of the latter expression.

2) Erosion modeling by means of either discrete or continuous hypotheses gives essentially equivalent results for surface recession over broad ranges of the problem parameters.

3) A simplified model for erosion of partially charred material, in which penetration depth is presumed to vary linearly with material density, is shown to be adequate for engineering calculations.

4) The application of simplified quasi-steady theory predicts recession rates which are low for a typical re-entry trajectory.

Appendix: Stability Limit for Explicit Iterative Solution of Eq. (5)

Taking Eq. (5) in the form

$$\frac{\partial \rho}{\partial t^*} = \dot{L}\frac{\partial \rho}{\partial y^*} - \sum_{i=1}^{N} \frac{(\rho - \rho_c)^{n_i}}{\rho_v}$$

$$A_i e^{-E_i/\Re T} = \dot{L}\frac{\partial \rho}{\partial y^*} - S(\rho)$$

and writing an "explicit" difference approximation about previous iterates

$$\frac{\rho_i^{(k)} - \rho_i^*}{\Delta t^*} = \dot{L}\frac{\rho_{i-1}^{(k-1)} - \rho_{i-1}^{(k-1)}}{2\Delta y^*} - S^{(k-1)}$$

Assuming an error $\epsilon^{(k)}$ in $\partial\rho/\partial t^*$ relative to the converged solution to the finite difference problem,

$$\epsilon^{(k+1)} \sim 0(\dot{L}\epsilon^{(k)}\Delta t/\Delta y^*)$$

where it is presumed that the contribution of the source term $S(\rho)$ to error growth or decay may be neglected. Qualitatively, amplification would therefore be expected to occur if $\Delta t > \Delta y^*/\dot{L}$. This was confirmed by means of numerical experiment and the explicit procedure was abandoned. (A similar result obtains if a fully explicit forward marching technique is applied.)

References

[1] Anfimov, N.A., "Heat and Mass Transfer Near the Stagnation Point with Injection and Suction of Various Gases Through the Body Surface," *Mekhanika Zhidkosti I Gaza,* Vol. 1, 1966, pp. 22-31.

[2] Gomez, A.V., Mills, A.F., and Curry, D.M., "Correlations of Heat and Mass Transfer for the Stagnation Region of Reentry Vehicle with Multicomponent Mass Addition," ASME Space Technology and Heat Transfer Conference, Los Angeles, Calif., June 1970.

[3] Lees, L., "Convective Heat Transfer with Mass Addition and Chemical Reactions," Third AGARD Colloquium on Combustion and Propulsion, Pergamon Press, New York, 1959.

[4] Mills, A.F. and Gomez, A.V., "The Effect of Gas Phase Chemical Reactions on Heat Transfer to a Charring Ablator," AIAA Paper 70-869, Los Angeles, Calif., June 1970.

[5] Bartlett, E.P., Nicolet, W.E., and Howe, J.J., "Heat-Shield Ablation at Superorbital Reentry Velocities," *Journal of Spacecraft and Rockets,* Vol. 8, May 1971, pp. 456-463.

[6] Edwards, D.K. and Balakrishnan, A., "Nongray Radiative Transfer in a Turbulent Gas Layer," *International Journal of Heat Mass Transfer,* Vol. 16, 1973, pp. 1003-1015.

[7] Quan, V., "Quasi-Steady Solution for Ablation-Erosion Heat Transfer," *Journal of Spacecraft and Rockets,* Vol. 7, March 1970, pp. 355-357.

[8] Munson, T.R. and Spindler, R.J., "Transient Thermal Behavior of Decomposing Materials, Part I:: General Theory and Application to Convective Heating," IAS Paper 62-30, IAS 30th Annual Meeting Seattle, Wash., 1962.

[9] Courtney, J.F., personal communication, April 1974, El Segundo, Calif.